

Original Article

VP3.15, a dual GSK-3 β /PDE7 inhibitor, reduces glioblastoma tumor growth though changes in the tumor microenvironment in a PTEN wild-type context

Maria Castello-Pons ^{a,g,1}, Maria A. Ramirez-Gonzalez ^{a,1}, Patricia Iglesias-Hernández ^{a,g},
 Nermina Logo Lendo ^b, Carlos Rodriguez-Martín ^c, Laura Quiralte ^b,
 Juan-Manuel Sepúlveda-Sánchez ^d, Olaya de Dios ^a, Carmen Gil ^{e,f}, Ana Martínez ^{e,f},
 Pilar Sánchez-Gómez ^{a,*}, Sergio Casas-Tinto ^{b,c,*}

^a Neurooncology Unit, Instituto de Salud Carlos III-UFIEC, Madrid, Spain

^b Instituto Cajal-CSIC, Avda. Doctor Arce 37, 28002 Madrid, Spain

^c Drosophila Models of Human Disease Unit, Instituto de Salud Carlos III-IIER, Madrid, Spain

^d Instituto de Investigaciones Biomédicas 1+12, Hospital 12 de Octubre, Madrid, Spain

^e Centro de Investigaciones Biológicas Margarita Salas-CSIC, Ramiro de Maeztu 9, 28040 Madrid, Spain

^f Centro de Investigación Biomédica en Red en Enfermedades Neurodegenerativas, (CIBERNED), Instituto de Salud Carlos III, Av. Monforte de Lemos, 3-5, 28029 Madrid, Spain

^g PhD Programme on Biomedical Sciences and Public Health, Universidad Nacional de Educación a Distancia, UNED-ISCIII 28040 Madrid, Spain

ARTICLE INFO

Keywords:

GSK-3 β

PDE7A

PTEN

GAL9

Tumor microenvironment

Macrophages

ABSTRACT

Glioblastoma (GB) is an incurable cancer of the brain, and there is an urgent need to identify effective treatments. This may be achieved by either identifying new molecules or through drug repurposing. To ascertain the therapeutic potential of known GSK-3 β and/or PDE7 inhibitors in GB, a drug screening was conducted using a *Drosophila melanogaster* glioma model. VP3.15, a dual inhibitor with anti-inflammatory and neuroprotective roles in multiple sclerosis, was selected for further investigation. VP3.15 demonstrated robust anti-tumor efficacy against a panel of human and mouse GB cells; however, its capacity to inhibit orthotopic growth was only observed in a wild-type PTEN cell line. The *in vivo* dependence on PTEN was further suggested with the results in fly gliomas. The analysis of the VP3.15-treated tissues revealed a notable reduction in the number of myeloid cells and in the degree of vascularization. Mechanistic studies indicate that VP3.15 diminishes the production of GAL9, a key molecule that stimulates pro-angiogenic macrophages. Our findings substantiate the pro-tumoral function of GSK-3 β , which might depend on the *PTEN* genetic status. Furthermore, we have delineated the therapeutic potential of VP3.15, which acts through the inhibition of the supportive role of the GB microenvironment. This molecule could be safely and effectively utilized after PTEN characterization in GB patients.

Introduction

Glioblastoma (GB), classified as a grade 4 astrocytoma, is one of the most aggressive forms of cancer, as well as the most frequent malignant primary brain tumor [1]. The standard treatment for GB is surgical removal of the tumor followed by radiotherapy and chemotherapy with temozolomide (TMZ). However, the invasiveness and proliferation rate of tumor cells, as well as their high resistance to conventional therapies favor the recurrence of GB, ultimately resulting in the death of the patients within 15–20 months after the initial diagnosis [1]. The

development of novel pharmacological agents, especially those capable of reaching the brain, is necessary to enhance the survival of these patients, who have not seen a therapeutic improvement in the last decades.

The aggressiveness of glioma cells is sustained by their close relationship with the surrounding stroma, particularly with the vascular and immune cells, the latter of which constitute up to 50 % of the tumor mass content in some cases of GB. Moreover, the immune compartment of GB is enriched with myeloid cells that possess strong immunosuppressive and pro-angiogenic properties [2]. Several groups have proposed that effectively eradicating glioma cells requires the targeting of these pro-tumoral

* Corresponding authors.

E-mail addresses: psanchez@isciii.es (P. Sánchez-Gómez), sergio.casas@isciii.es (S. Casas-Tinto).

¹ These authors contributed equally.

myeloid cells as well. However, thus far none of the proposed molecules has achieved clinical success [3]. In a similar manner, anti-angiogenic strategies have been unsuccessful in prolonging the overall survival of patients with GB to date [4].

Notwithstanding the above, there is a consensus that genes regulating the interaction between glioma cells and the surrounding microenvironment remain important as therapeutic targets. That is exemplified by *PDE7B* [5] and *GSK-3 β* [6]. Indeed, overexpression of *PDE7B* has been observed in GB, resulting in enhanced tumor growth and aggressiveness in murine models [5]. Furthermore, the elevation of intracellular cAMP levels through the inhibition of cAMP phosphodiesterases with various *PDE2/4/7* inhibitors may prove to be a beneficial therapeutic strategy, leading to the suppression of glioma cells [7,8]. Likewise, emerging evidence suggests that *GSK-3 β* functions as a tumor promoter in glioma, playing a key role in proliferation, resistance to radio-chemotherapy, and activation of invasion [9,10]. Moreover, the inhibition of *GSK-3 β* with small molecules has been demonstrated to enhance the effect of TMZ in glioma cells and to reduce GB growth *in vivo* [11,12].

Our research group has extensive experience in the design and development of *GSK-3 β* and *PDE7* inhibitors, primarily for CNS diseases [13–15]. This includes the development of the first dual *GSK-3 β /PDE7* inhibitors described to date [16]. In this study, we screened a diverse range of chemically distinct small molecule inhibitors of *GSK-3 β* , *PDE7* and/or dual *GSK-3 β /PDE7* in a *Drosophila melanogaster* glioma model with the objective of identifying the most promising candidates for future translational studies. We selected VP3.15, an iminothiadiazol dual inhibitor of the two targets, based on its superior anti-tumor capacity. *In vitro* viability tests using different GB models confirmed its potential for chemotherapeutic treatment. However, in orthotopic xenografts and allografts, the effect of VP3.15 was limited to the inhibition of the growth of a *PTEN* wild-type GB, accompanied by a reduction in tumor vascularity. This *PTEN* dependency was subsequently validated in *Drosophila melanogaster* models of glioma. The results of the mechanistic studies indicate that the effect of VP3.15 in the presence of *PTEN* is mediated through a reduction in Gal9 expression and the consequent inhibition of the recruitment of pro-tumoral macrophages. In conclusion, the presented results indicate that VP3.15 may serve as a highly efficacious inhibitor of *PTEN*wt glioma growth, influencing the interaction between tumor cells and their supportive microenvironment.

Materials and methods

Drug synthesis and purification

All the compounds were synthesized, isolated, purified and characterized in CIB-CSIC laboratories following previously described procedures. Table S1a shows the chemical structure, the IC₅₀ values against their targets and the reference for their synthetic procedure.

In vivo assays

Drosophila melanogaster UAS/GAL4 expression binary system

We used the binary expression system Gal4/UAS to modulate gene expression. Briefly, the *Gal4* transcriptional activator from *Saccharomyces cerevisiae* was expressed under the control of a specific promoter active in specific tissues or cells. We used *repo*, a regulatory sequence that controls the expression of the gene *reverse polarity* and is active specifically in glial cells [17]. Next, the activating sequence *UAS* (*Upstream Activating Sequence*) was fused to a gene of interest. By crossing two parental lines, one carrying the gene of interest fused to the *UAS* sequence, and the other one containing the gene encoding *GAL4* under the control of a tissue-specific promoter, the offspring activates the expression of the gene or dsRNA of interest in a specific tissue [18].

Drosophila stocks

Fly stocks were maintained at 25 °C, 60 % humidity and 12/12 h light/dark cycles. Fly stocks used were *UAS-LacZ* (BL8529), *UAS-myrRFP* (BL7119), *repo-Gal4* (BL7415), *dnc-GFP* MiMIC (BL43732), *UAS-GSK3^{DN}* (BL5359), *UAS-dnc RNAi* inserted in chromosome III (BL27250) and *UAS-PTEN RNAi* (BL25841) from the Bloomington Stock Center (<https://flystocks.bio.indiana.edu/>). The stocks *UAS-dnc RNAi* inserted in chromosome II (VDRc 107967) and *UAS-GSK3 RNAi* (VDRc 101538) from VDRc (https://shop.vbc.ac.at/vdrc_store/), and *UAS-dp110CAAX* and *UAS-EGFR* gifted by R. Read [19].

GB model was generated as previously described [19]. Briefly, we used the specific pan-glial promoter *repo* to express the constitutively active forms of *EGFR* and *PI3K* in glial cells and precursors, under the control of the *UAS/Gal4* system. This genetic combination has been proved to reproduce GB features in *Drosophila* brain and is a well established model [19–21]. In addition, we expressed a myristoylated form of the *red fluorescent protein* (*UAS-myrRFP*) under the control of *repo-Gal4* to visualize the membrane of glial/GB cells.

Drug screening

The drugs were administered to *Drosophila* larvae through the diet mixed with the food. The drugs were diluted in dimethyl sulfoxide (DMSO) to a final concentration of 50 mM–200 mM according to their solubility:

VP3.15 and VP1.14 were dissolved at 100 mM, VP1.15, S14, TC3.6, TDZD8, Tideglusib and VP2.51 at 200 mM and VP0.7 was dissolved at 50 mM due to challenges in achieving complete dissolution. Even if VP07 was not fully dissolved in DMSO, we decided to incorporate it into the experiments.

The diluted compounds were mixed into standard food heated at 56 °C, a temperature at which it remains in liquid form, enabling the mixture of the compound with the food.

We prepared 5 mL of food mixed with 5, 20, or 35 μ l of each compound. The highest DMSO concentration was found to be toxic to the larvae so 5 and 20 μ l amounts were tested.

Drosophila Larval brain dissection and immunostaining

We dissected the larvae in phosphate buffered saline (PBS). We held the head of the larva with tweezers, and we inserted forceps through the opening of the section. Next, we pushed until the internal wall and viscera were exposed to the exterior. Finally, the viscera of the larva were removed, and the brain was located and separated from the rest of the body.

We fixed *Drosophila* tissues with 4 % formaldehyde (PFA) for 20 min at room temperature (RT). Next, we washed the samples three times in PBS 1x + 0.3 % Triton X-100 (PBT) for 10 min under stirring at RT. Next, we blocked the samples in (0.3 % PBT + 5 % BSA) under agitation for 30 min at RT. We incubated the primary antibody in blocking solution at 4 °C overnight. Next, we washed the samples in PBT (3 \times 15 min) and we incubated the secondary antibody (fluorochrome-conjugated) in blocking solution for 2 h in the dark and under constant agitation at RT. Finally, we washed the samples in PBT (3 \times 15 min) and we mounted the brains on microscope slides, using mounting medium (Vectashield with DAPI), and covering the slide with a coverslip until analysis.

We used the primary antibody anti-Repo (DSHB, 1/100), which recognizes the transcription factor encoded by the *repo* gene, to mark the nuclei of glial cells.

Secondary antibodies (ThermoFisher): anti-mouse Alexa 488. DNA was stained with 2-(4-amidinophenyl)-1H-indole-6-carboxamide-Dine (DAPI) at 1 μ M in Vectashield mounting media (Vector Laboratories).

Drosophila GB quantification and analysis

Drosophila brain samples were mounted in Vectashield with DAPI and we acquired confocal images using a 20x or 40 \times oil objectives, 1024 \times

1024 resolution, and images were taken every micrometer in Z sections. We visualized the number of normal glia (controls) or transformed glia (GB samples) cells with the anti-repo staining. To quantify GB progression, we counted the number of repo positive cells per brain hemisphere using IMARIS (Bitplane) software. Each point represents the number of repo-positive cells in one hemisphere of the brain.

GB cells

We used 4 mouse and two human GB cell lines (Fig. 3a). The SVZ-wt and SVZ-vIII cell lines were previously characterized in our laboratory [22]. They were derived from p16/p19 ko subventricular zone (SVZ) progenitors after the overexpression of EGFRwt or the deleted isoform EGFRvIII. Even though they were generated from C57/BL6 mouse tissue they need to be injected into immunodeficient mice to generate tumors. GL261 cells were acquired commercially and NPE-IE cells were kindly donated by Stephen Pollard [23]. These two cell lines form tumors when injected into immunocompetent C57/BL6 mice. 12O89 cells were derived from a patient's sample after subject's written consent (according to the Declaration of Helsinki) and with the approval of the Ethical Committee at Hospital 12 de Octubre (Madrid, Spain) (CEI-18/024). RG1 cells were kindly donated by Dr. Rosella Galli [24]. Both human cells form tumors when injected into the brains of Nude mice. All cells express the Luciferase gene as a reporter to monitor tumor growth *in vivo*.

All the cells were maintained in Complete Medium (DMEM/F12 (Thermo Fisher Scientific) supplemented with B27 (1:50) (Thermo Fisher Scientific); penicillin-streptomycin (1:100) (Lonza); 0.4 % heparin (Sigma-Aldrich); and 40 ng/ml EGF and 20 ng/ml bFGF2 (Peprotech). They were maintained at 37 °C/5 % O₂ and passaged after enzymatic dissociation using Accumax (Millipore).

Orthotopic mouse glioma models

Animal experiments were reviewed and approved by the Research Ethics and Animal Welfare Committee at our institution (Instituto de Salud Carlos III, Madrid) (PROEX 055/19), in agreement with the European Union and national directives. The tumors were established after the injection of 50,000–300,000 cells (depending on the cell line) in 2 µl of complete medium with a Hamilton syringe into the brains of C57/BL6 mice (for NPE-IE and GL261 cells) or Nude mice (for the rest). The injections were made into the following coordinates: A–P, –0.5 mm; M–L, +2 mm, D–V, –3 mm (related to Bregma) using a Leica Stereotaxic device. Three days after the tumor implantation, animals started receiving treatment. For that, the stock of VP3.15 (100 mg/ml in DMSO) was further dissolved in 5 % Trocrisolve (Tocris) in saline and injected intraperitoneally (i.p.) (10 mg/kg/day, 5 days/week). Control animals were treated with 5 % Trocrisolve in saline. For intravenous treatment, the stock of VP3.15 was dissolved in saline and injected 2 days/week (5 mg/kg). For subcutaneous treatment the stock of VP3.15 was dissolved with 5 % Trocrisolve in saline and injected 5 days/week (30 mg/kg). TMZ (MedChemExpress) was dissolved in PBS 1 % BSA and injected i.p. (5 mg/kg/day, 5 days/week). Tumor growth was monitored by bioluminescence in an IVIS equipment (PerkinElmer) after intraperitoneal injection of D-luciferin (75 mg/kg; Thermo Fisher Scientific). Animals were sacrificed when they showed signs of disease, the brains were dissected out and processed for cellular and molecular analysis.

In vitro treatment

For viability testing, 5000 cells were seeded in triplicate in 96-well plates. After 24 h, cells were treated with VP3.15 (at the indicated concentrations) and viability was measured after 72 h of treatment using Alamar Blue (Thermo Fisher Scientific). For that, the Alamar Blue reagent was added to the cell media (1:10) and Absorbance at 570 nm (using 600 nm as a reference wavelength) was measured in a TECAN equipment (Life Sciences). For all cell lines, the absorbance of each well was related to that of the controls, which were treated with DMSO (1:1000).

Immunohistochemical (IHC) staining and quantification

Mouse brains were fixed in 4 % PFA, embedded in paraffin and sectioned (5 µm) in a microtome (Leica). For IHC staining with different antibodies (Table S1b), the slides were preheated for 30 min at 65 °C, and the BOND RXm automated advanced staining system (Leica Biosystems) programmed with the specific protocols (Table S1c). All the stained slides were scanned using the NanoZoomer-SQ microscope slide digitizer (Hamamatsu). QuPath software was used for the quantification, setting two different methods depending on the specific antibody: positive-cell detection (for Ki67 staining) and pixel classification (for Endomucin, CD68 and CD206 staining). The first one measures the percentage of positive cells with respect to negative cells in a specific area. In the second one an intensity threshold was established in the regions of interest for each specific marker. Signal above that threshold was considered positive and the percentage of positive staining related to the total area was calculated. Table S1d provides detailed information on the parameters and settings employed in all quantifications.

Quantitative reverse-transcriptase PCR (qRT-PCR)

Frozen samples of the tumor tissue were used for RNA extraction, which was performed using the RNA isolation Kit (Roche). Equivalent amounts (1 µg) of purified RNA were reverse transcribed using Prime-Script RT Reagent Kit (Takara) and quantitative real time PCR (qRT-PCR) reactions were performed using the Light Cycler 480 (Roche Diagnostics) with the SYBR Premix Ex Taq (Takara) and specific primers for each gene (Table S1b). Relative gene expression was calculated using the double delta Ct method.

Western Blot (WB) analysis

Protein extracts from cell pellets or glioma tissue samples were prepared by resuspending them in lysis buffer (50 mM Tris (pH 7.5), 300 mM NaCl, 0.5 % SDS, and 1 % Triton X-100), followed by 15 min (100 °C) incubation. The lysed extracts were centrifuged at 13,000 g for 10 min (RT) and the protein content was determined using the BCA Protein Assay Kit (Thermo Fisher Scientific). 30 µg of protein were resolved by 12 % SDS-PAGE and then transferred to a nitrocellulose membrane (Hybond-ECL, Amersham Biosciences). The membranes were blocked and then incubated with the primary (1 h at RT) and the respective secondary antibody (2 h at RT) (Table S1b) diluted in TBS-T (10 mM Tris-HCl (pH 7.5), 100 mM NaCl, and 0.1 % Tween-20). Proteins were visualized by enhanced chemiluminescence with ECL (Pierce) using the Imager 800 (Amersham Biosciences) and the signal was quantified by ImageQuant TL software (Cytiva).

In silico analyses

The generation of the single-cell transcriptomic (scRNAseq) integrated atlas has been previously described [25]. In summary, we downloaded different scRNAseq databases available in public repositories of normal brain [26], lower grade gliomas (LGG), and GB both newly diagnosed and recurrent [27]. Subsequent data processing and analysis were performed using Seurat package v4.3.0. Batch-corrected dimensionality reduction was performed using Harmony [28], correcting for sample type. Cell types were manually identified based on the canonical markers described in previous studies and confirmed by scCATCH (single cell Cluster-based Annotation Toolkit for Cellular Heterogeneity) [29].

To analyze and visualize the correlation between *GSK3b* and *PDE7A/B* expression, we used the GlioVis data portal (<http://gliovis.bioinfo.cnio.es>) and the TCGA (The Cancer Genome Atlas) and the CGGA (Chinese Glioma Genome Atlas) cohorts (including GB and LGG).

Statistical analysis

Data presentation and statistical analysis was performed using GraphPad Prism 5 software. Differences between pairs of experimental

groups were analyzed by two-tailed un-paired Student's *t*-test and one-way ANOVA. To assess survival differences in mouse experiments we used the Kaplan–Meier method, evaluated with a two-sided log-rank test. *P* values < 0.05 were considered significant (**p* < 0.05; ***p* < 0.01; ****p* < 0.001; *****p* < 0.0001; n.s., non-significant). All quantitative data presented are the mean ± SEM.

Results

PDE7 and GSK-3β expression in GB patients

We conducted an *in silico* analysis integrating publicly available data from scRNAseq studies of non-tumoral brain and gliomas [26,27] with a focus on the analysis of *PDE7* and *GSK-3β* expression in gliomas. The analysis revealed the presence of distinct immune (macrophages, microglia and T cells), astrocytic and vascular (endothelial cells and pericytes) cell groups (Fig. 1a-left). The analysis of *PDE7B* and *GSK-3β* transcription showed that both genes were expressed in various cell types within the normal brain. However, a notable increase in *PDE7B* and *GSK-3β* expression was observed in GB samples compared to LGG (Fig. 1a-right). In GB, *PDE7B* transcription is predominantly observed in astrocytic cells (including neoplastic cells) and pericytes, whereas *GSK-3β* is expressed in a ubiquitous manner (Fig. 1a-right). Subsequently, we examined the correlation between *GSK-3β* and *PDE7A* or *PDE7B* expression levels in the Gliovis database. The results demonstrate a robust positive correlation (Fig. 1b) (*p*-value = 0.00 in both cases), suggesting that the elevation of *GSK-3β* and *PDE7* occurs concurrently.

Relevance of GSK-3 and PDE7 in the *Drosophila* GB model

To ascertain the role of GSK-3 and PDE7 in the progression of glial tumors *in vivo*, a GB model in *Drosophila melanogaster* [19,21] was employed. The expression of *dunce* (*dnc*), the orthologue of *PDE7* in flies, was determined in *Drosophila* larvae bearing a GB. We used a green fluorescent protein reporter (*dnc-GFP*) to monitor the activity of *dnc* promoter. Confocal images of the brain lobes showed an increase in the GFP signal in GB samples suggesting that *dnc* expression is upregulated in GB brains in *Drosophila* (Fig. 1c).

Next, to ascertain the functional contribution of *GSK-3* and *dnc* to GB progression, the number of glial cells per brain lobe was counted in WT, GB flies, and GB flies upon *GSK3* or *dnc* knockdown (RNAi) or the expression of *GSK-3* dominant negative (DN) forms. The results show that the interference with *GSK-3* and *dnc* expression or function markedly reduces the number of cells in the GB (Fig. 1d). Subsequently, we examined the lethality resulting from the induction of a GB in larvae. The results show that the lethality induced by the induction of a GB in fly larvae can be rescued by the knockdown of *GSK-3* or *dnc* in GB cells (Fig. 1e). These findings suggest that *GSK-3* and *dnc* are necessary for GB progression *in vivo*, making them promising candidates for therapeutic intervention in these tumors.

Drug screening in the *Drosophila* GB model

Next, anti-GB effect of a number of chemically diverse GSK-3 and PDE7 inhibitors was evaluated. These compounds had been previously designed and synthesized in our laboratory as pharmacological tools to modulate specifically these two targets (Table S1a). Therefore, a selection of four GSK-3, three PDE7 inhibitors, and three multitarget compounds [14], capable of inhibiting both GSK3 and PDE7 (Table S1a), was chosen for further analysis. The anti-GB effects of these ten drugs were evaluated at two distinct concentrations. A total of 5 μl and 20 μl of each compound stock, including a control containing only DMSO, were added to 5 ml of fly food. The viability of the flies was assessed, and the number of glial cells was counted. The genetically-induced GB co-expresses the gene for red fluorescent protein (*UAS-myrRFP*). This enables the selection of brains containing glial tumors (red fluorescence positive) and the

enumeration of glial cells stained with the specific antibody repo (Fig. 2a). The compounds (Table S1a) VP3.15, TC 3.6, S14, TDZD8, Tideglusib and VP 0.7 significantly reduced the number of glial cells in GB. The administration of high concentrations of TDZD8 (20 μl) and VP 2.51 (5 μl and 20 μl) resulted in lethal outcomes. Conversely the addition of VP 1.14, VP 1.15 and TC 3.6 did not elicit a notable impact on the number of glial cells within the brains of the flies (Fig. 2b and c).

The findings suggest that our GSK3 inhibitors may prove more efficacious than the PDE7 inhibitors in preventing the progression of GB in *Drosophila*. Moreover, dual inhibition of these two targets by compound VP3.15 resulted in a significant impairment of GB growth at both concentrations tested. This drug was selected for further investigation of its potential to inhibit GB progression.

Effect of VP3.15 in the *in vitro* and *in vivo* growth of mouse and human GB cells

To further examine the anti-tumor capacity of VP3.15, we initially conducted a viability assay on a panel of primary GB cells derived from human or mouse GB tumors with diverse genetic characteristics (Fig. 3a). The cell cultures were incubated for three days in the presence of increasing concentrations of the compound and the viability was measured with Alamar Blue. While there were some differences in the sensitivity of each individual cell line, a significant decrease in the viability was observed in all of them in the presence of 2 μM of VP3.15 compared to the control (cells treated with the vehicle DMSO) (Fig. 3b and c).

Next, to validate these results *in vivo*, we injected the GB cell lines into the brain of mice that were then treated systemically with 10 mg/kg of VP3.15 (i.p. injections). We analyzed the overall survival of the animals, and the results show that the drug did not inhibit the growth of GL261 (Fig. 4a), NPE-IE (Fig. 4b) or 12O89 (Fig. 4c) cells *in vivo*. However, *in situ* imaging and Kaplan-Meier curves showed a significant reduction in the tumor growth of SVZ-vIII GB cells (Fig. 4d and e). To determine whether the route of administration is relevant for this anti-tumor effect, we tested the compound by intragastric or intravenous administration. The results suggest that using different routes of drug administration did not improve the overall survival of SVZ-vIII treated with VP3.15 (Fig. S1a). Furthermore, we did not find a synergism between VP3.15 and TMZ, the standard GB treatment (Fig. S2).

Closed examination of the tumors formed in the mouse brains revealed an apparent reduction in the amount of hemorrhage after VP3.15 treatment in SVZ-vIII, but not in GL261 tumors (Fig. 5a). Consequently, the IHC analysis of the tumor sections confirmed a reduction in the endomucin staining, which marks endothelial cells, in SVZ-vIII (Fig. 5b) but not in GL261 (Fig. 5c) tumors in the presence of the drug. Notably, we did not observe any changes in the number of proliferating cells in SVZ-vIII tumors treated with VP3.15 (Fig. S3).

The presence of wild-type PTEN is necessary for the anti-tumor effect of VP3.15

Recent publications suggest that gliomas deficient for the tumor suppressor *PTEN* show a strong inhibition of GSK-3β, which in turn induces the expression of galectin *Gal9* [30]. Notably, the main difference between SVZ-vIII and the other tumors that were not sensitive to VP3.15 is the presence of wild-type *PTEN* (Fig. 3a). To address the relevance of *PTEN* in the response of GB cells to this inhibitor, we knocked down *Pten* expression in GB cells in the *Drosophila* glioma model using a specific *UAS-Pten RNAi* transgenic line. Fig. 6a shows that the reduction in the number of GB cells in VP3.15 treated flies was reversed in GB + *PtenRNAi* flies. Therefore, the results suggest that the anti-GB activity of VP3.15 in *Drosophila* is *Pten* dependent, although we cannot discard that other factors contribute to the specific anti-tumor response observed in the SVZ-vIII tumors.

In mouse models, we observed a significant downregulation of *Gal9* transcription (Fig. 6b) and protein accumulation (Fig. 6c) in SVZ-vIII

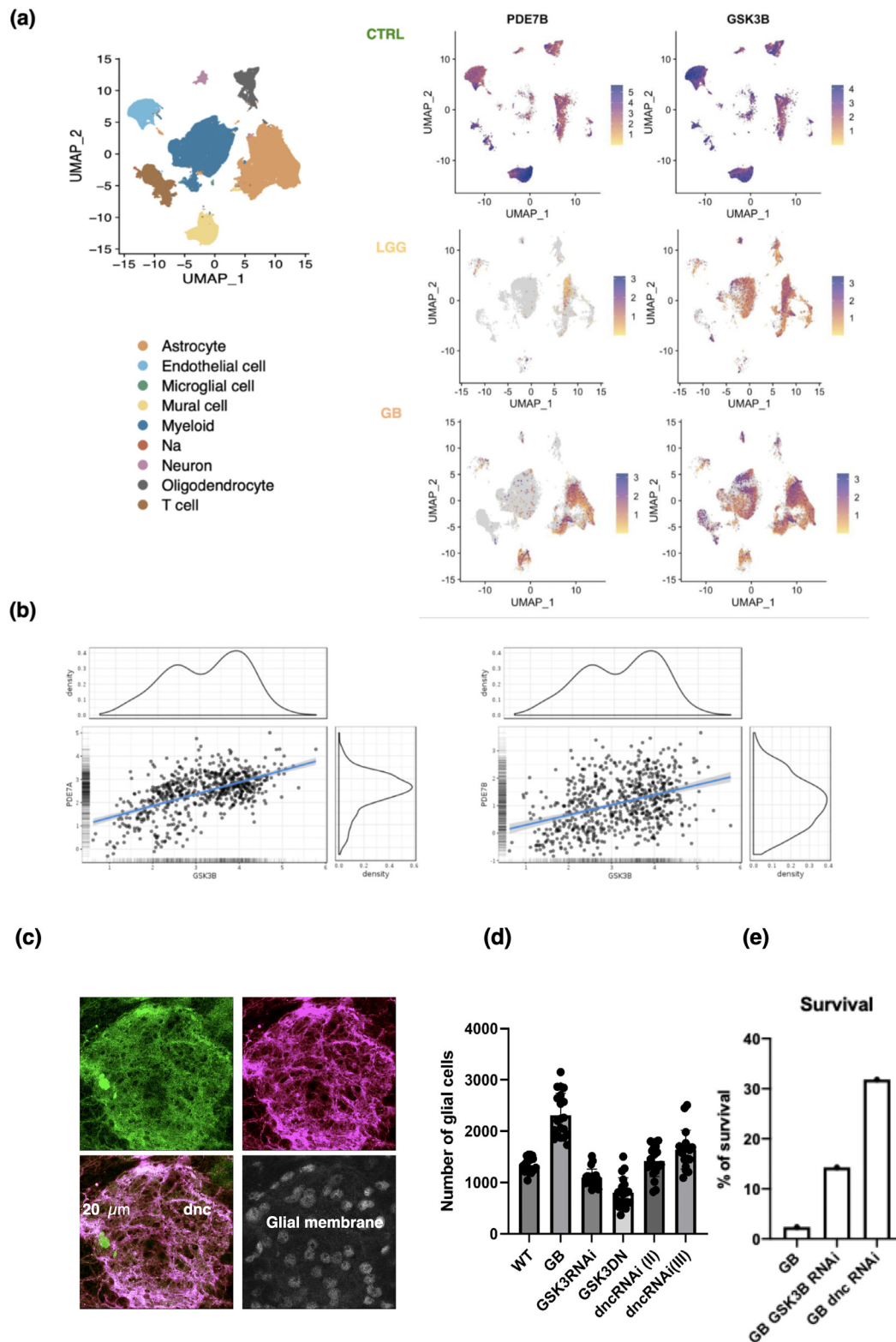


Fig. 1. Analysis of *GSK3B* and *PDE7* expression in GB. **a**) UMAP plot annotated according to each cell type of the integrated object (control and glioma scRNAseq databases). **b**) UMAP plot of cells with positive *PDE7B* and *GSK3B* expression in normal brain (CTRL), lower grade gliomas (LGG) and glioblastomas (GBM). **c**) Data from Gliovis database (<http://gliovis.bioinfo.cnio.es/>) showing the correlation of *GSK3B* expression with *PDE7A* or *PDE7B* in the CCGA (Chinese Glioma Genome Atlas) cohort of gliomas. **c**) Amplification of confocal images showing brain tissue from *Drosophila melanogaster* bearing a genetically induced GB. Dunc (dnc) is the PDE orthologue in *Drosophila* (shown in green) is upregulated in GB tissue (GB membrane in red, and GB cells nuclei in gray). **d**) Graphic showing the number of GB cells in *Drosophila* upon *GSK3* or *dnc* knockdown (RNAi) or dominant negative expression *GSK3*^{DN}. **e**) Survival of flies reaching adulthood upon GB induction, GB and *GSK3* or *dnc* knockdown by RNAi.

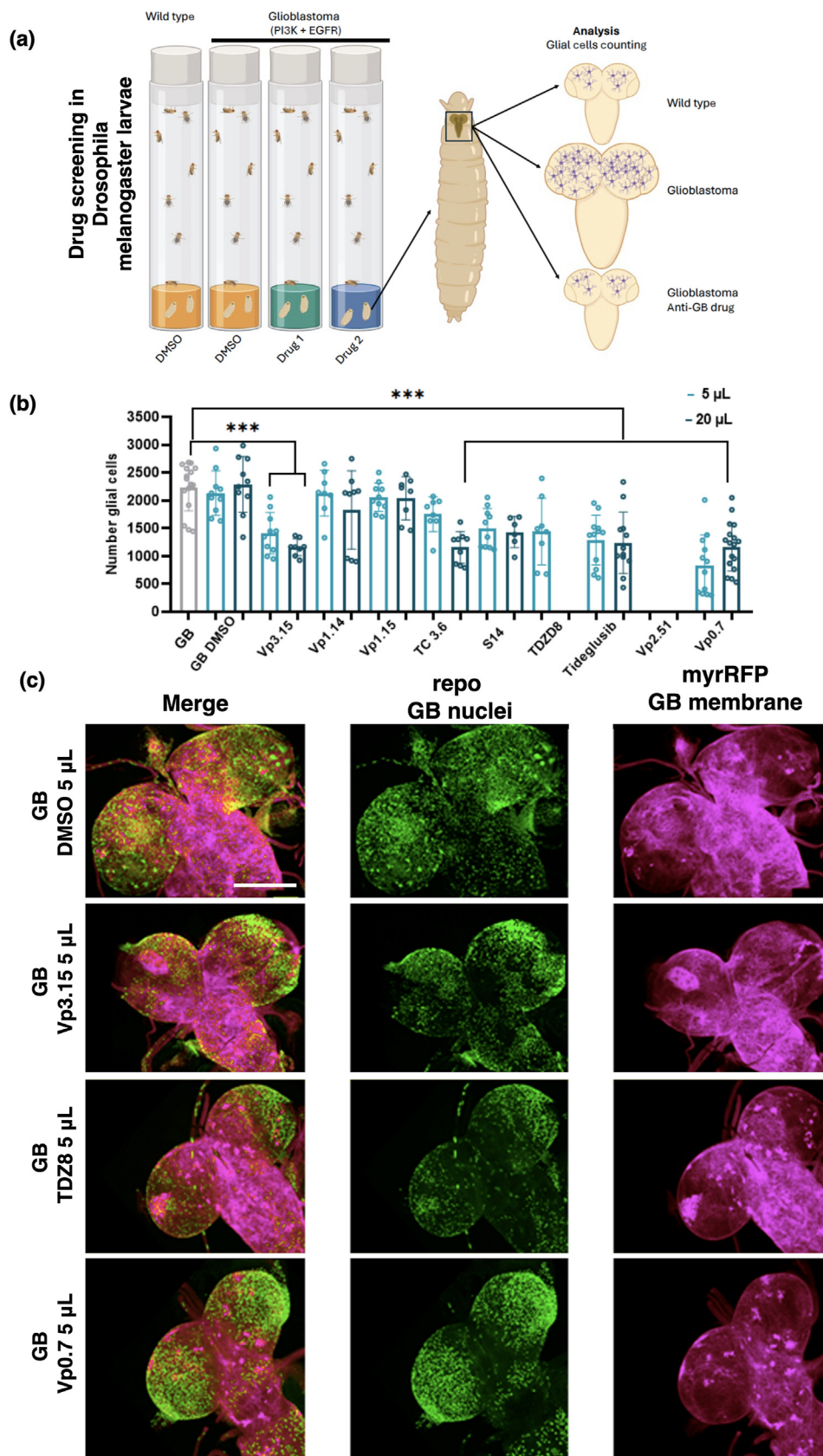


Fig. 2. Drug screening in *Drosophila* larvae. a) Schematic representation of drug screening performed in *Drosophila melanogaster* larvae. Drugs were mixed in the food using 5, 20 or 35 μ l per 5 ml. b) Graph showing the number of GB cells per brain lobe treated with vehicle (dimethyl sulfoxide, DMSO) of drugs. c) Representative images of *Drosophila* larvae brains with a genetically induced GB treated with 5 μ l of DMSO, VP3.15, TDZ8 or VP0.7. Glial cells are marked in red (myr-RFP) and nuclei of all cells is marked in blue (DAPI). Scale bar: 100 μ M.

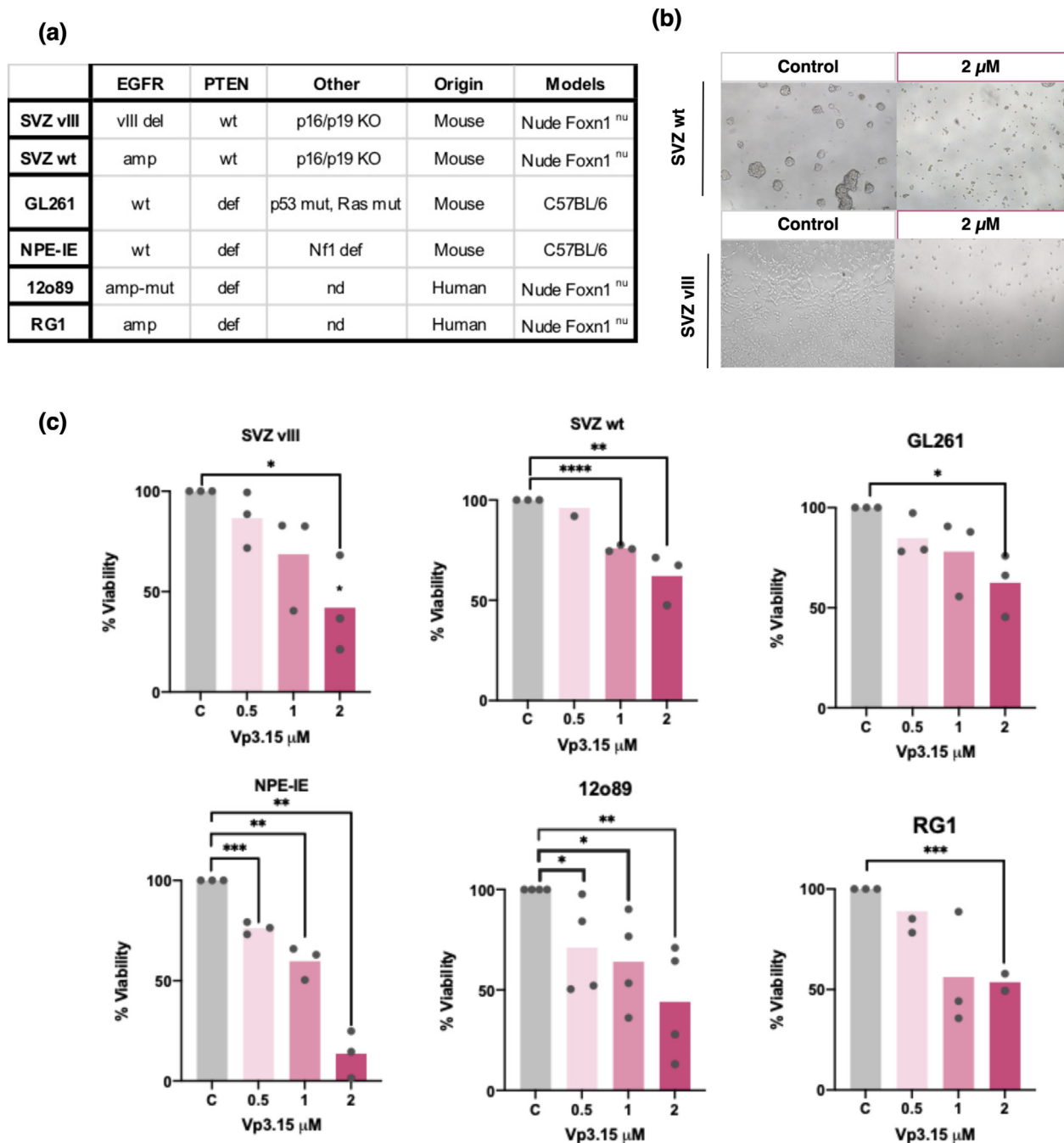


Fig. 3. *In vitro* response of GB cells to Vp3.15. **a)** The table displays the list of GB cells used in this study, along with their known genetic features, their origin (human or mouse tumors), and the mice that are used to grow them *in vivo* after orthotopic implantation (Models). **b)** Representative contrast-phase images of two distinct GB cell lines treated either with dimethyl sulfoxide (DMSO) (control) or VP3.15 at 2 μ M over a 72-h period. **c)** The various cell lines were grown in the presence of DMSO (1:1000) or increasing concentrations of VP3.15. Following a 72-h incubation period, the viability of the cells was determined by measuring the absorbance after incubation with Alamar Blue. The absorbance measured in the presence of DMSO was designated as 100 %. The experiment was repeated 3 times. * $P \leq 0.05$; ** $P \leq 0.01$; *** $P \leq 0.001$; **** $P \leq 0.0001$. del: deletion, amp: amplification, wt: wild-type, mut: mutant, def: deficient, KO: knock out, nd: not determined.

tumors treated with VP3.15, but not in GL261 tumors (Fig. 6b and c). To further analyze the effect of the inhibitor on Gal9, we treated GL261 and SVZ-vIII cells in the presence of 1 μ M of VP3.15 and analyzed the levels of different proteins at different time points. Consistent with published results, the level of Gal9 expression was significantly higher in the PTEN-deficient GL261 cells (Fig. 6d). We observed a reduction in the amount of Gal9 protein 24 h after the exposure of SVZ-vIII cells to VP3.15. We also observed a similar trend in GL261 cells treated with VP3.15, although the remaining levels of Gal9 protein were higher in the PTEN-proficient GB cell line (Fig. 6d).

Galectins are involved in the modulation of cell-cell and cell-matrix interactions. Specifically, secreted Gal9 recruits macrophages that, once inside the tumor tissue, promote GB angiogenesis and growth [30]. Indeed, there is a highly significant correlation between the expression of *LGALS9* (the gene encoding Gal9) and *CD68* (a classical marker of GB macrophages) expression in patient samples from two distinct glioma cohorts (Fig. S4a). Moreover, the scRNAseq integrated atlas (Fig. 1a) was employed to elucidate the pattern of expression of *LGALS9*. Our findings revealed that in the tumors, this gene is expressed extensively, particularly in myeloid cells, yet also to a lesser extent in glial cells. This suggests

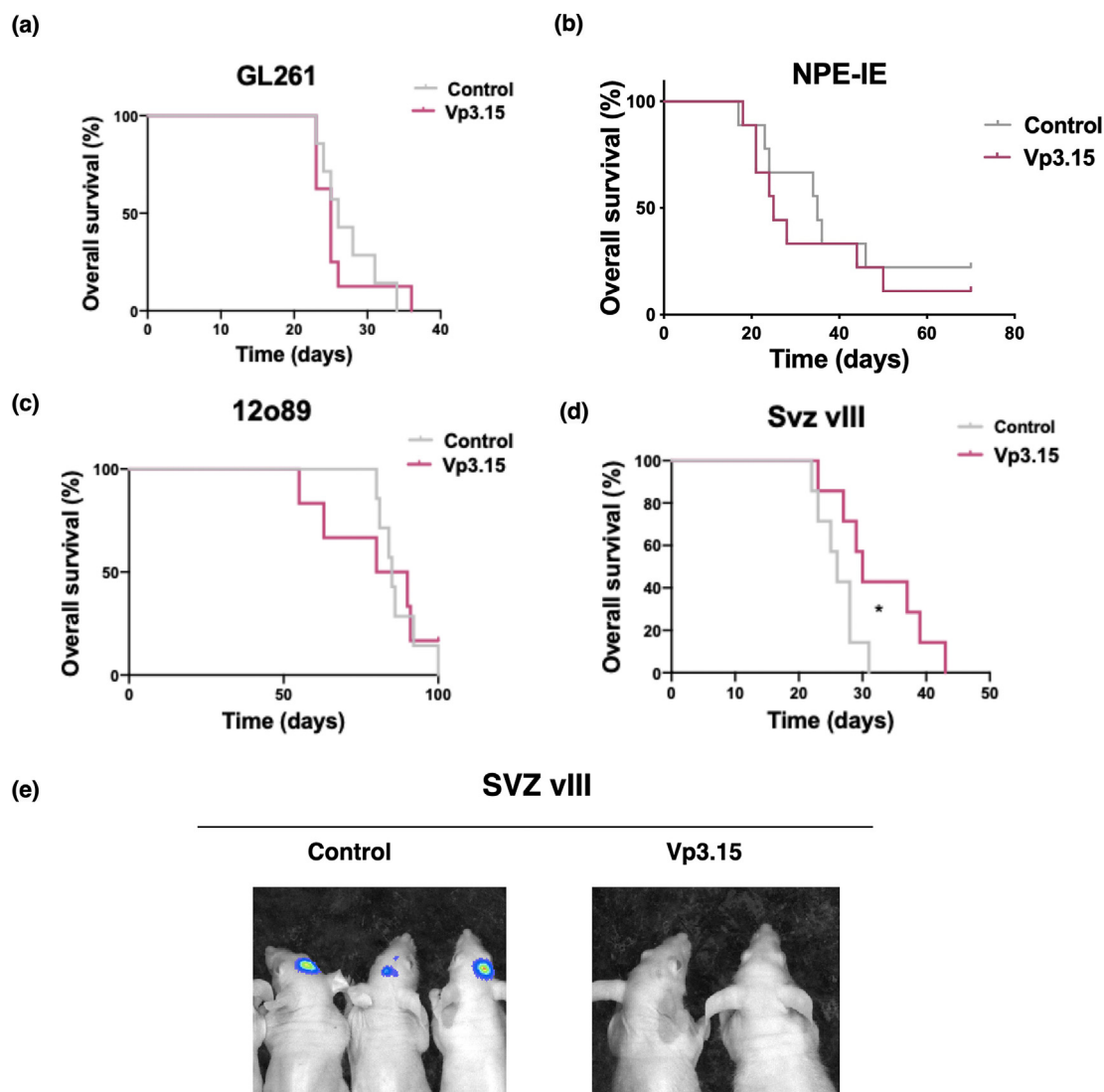


Fig. 4. *In vivo* analysis of the effect of VP3.15 in GB. a-d) Kaplan-Meier overall survival curves of mice that were orthotopically implanted with GL261 (a), NPE-IE (b), 12O89 (c) or SVZ-vIII (d) cells. The animals were administered i.p. injections of the vehicle (control) or VP3.15 (10 mg/kg/day, 5 days/week), and they were sacrificed when they exhibited symptoms of the disease ($n = 7$). (e) Representative image of the bioluminescence analysis of animals two weeks after the injection of SVZ-vIII cells, which express the luciferase reporter. * $P \leq 0.05$.

that multiple cell types may be capable secreting this molecule (Fig. S4b). These observations led us to hypothesize that VP3.15 may influence the population of macrophages within the tumors. To explore this possibility, we quantified the number of myeloid cells through IHC in mouse xenograft GB sections. The results show a significant reduction in the percentage of CD68 (Fig. 7a) and CD206 (Fig. 7b) (a marker of M2 protumoral macrophages [31]) positive cells, in SVZ-vIII tumors treated with VP3.15, but not in GL261 gliomas (Fig. 7c and d). In addition, the expression of *CD206* (measured by qRT-PCR was reduced SVZ-vIII, but not in GL261 tumors treated with the VP3.15 (Fig. 7e). Collectively, these results demonstrate that the anti-tumor effect of VP3.15 in a PTENwt GB is mediated, at least in part, by reducing the recruitment of pro-angiogenic macrophages.

Discussion

GB is one of the most lethal tumors with a very short life expectancy at diagnosis. Currently, there is no effective treatment, mainly due to its highly heterogeneous and plastic nature [2]. GB is a multifactorial disease and in consequence, combination of different drugs are emerging as promising therapeutic approaches. In any case, there is an urgent need to

search for new therapeutic strategies, particularly those that could impair the supportive function of the GB microenvironment.

VP3.15 is a small heterocyclic drug-like molecule with safety profile and good pharmacodynamic and pharmacokinetic properties after intraperitoneal administration in different *in vivo* models [32]. Interestingly, it has shown neuroprotection of retinal cells both *ex vivo* and *in vivo* in a model of retinitis pigmentosa [33,34], and neuroprotective and anti-inflammatory properties in models of multiple sclerosis and experimental autoimmune encephalomyelitis [34–36]. Here, we show that VP3.15 inhibits the growth of GB cells *in vitro*, arguing for an anti-proliferative contribution of the drug. Indeed, several groups have shown the cytotoxic effects of GSK-3 blockade, either genetically or with small molecules, in gliomas [37–39]. In spite of the inhibitory action of the PI3K/AKT pathway, commonly hyperactivated in GB, on GSK-3 β , most of the previous studies establish a general oncogenic role for GSK-3 β in these tumors [37,38]. GSK-3 β expression is upregulated in GB [40,41], and activating phosphorylation at Tyr216 is present in GB samples [39]. Thus, GB cells show activation of GSK-3 β despite the inhibitory effect of GSK-3 β ^{Ser9} phosphorylation by the PI3K/AKT pathway. This could be explained by the action of additional pathways to prevent GSK-3 β ^{Ser9} phosphorylation, as it has been previously proposed [42]. Moreover, it

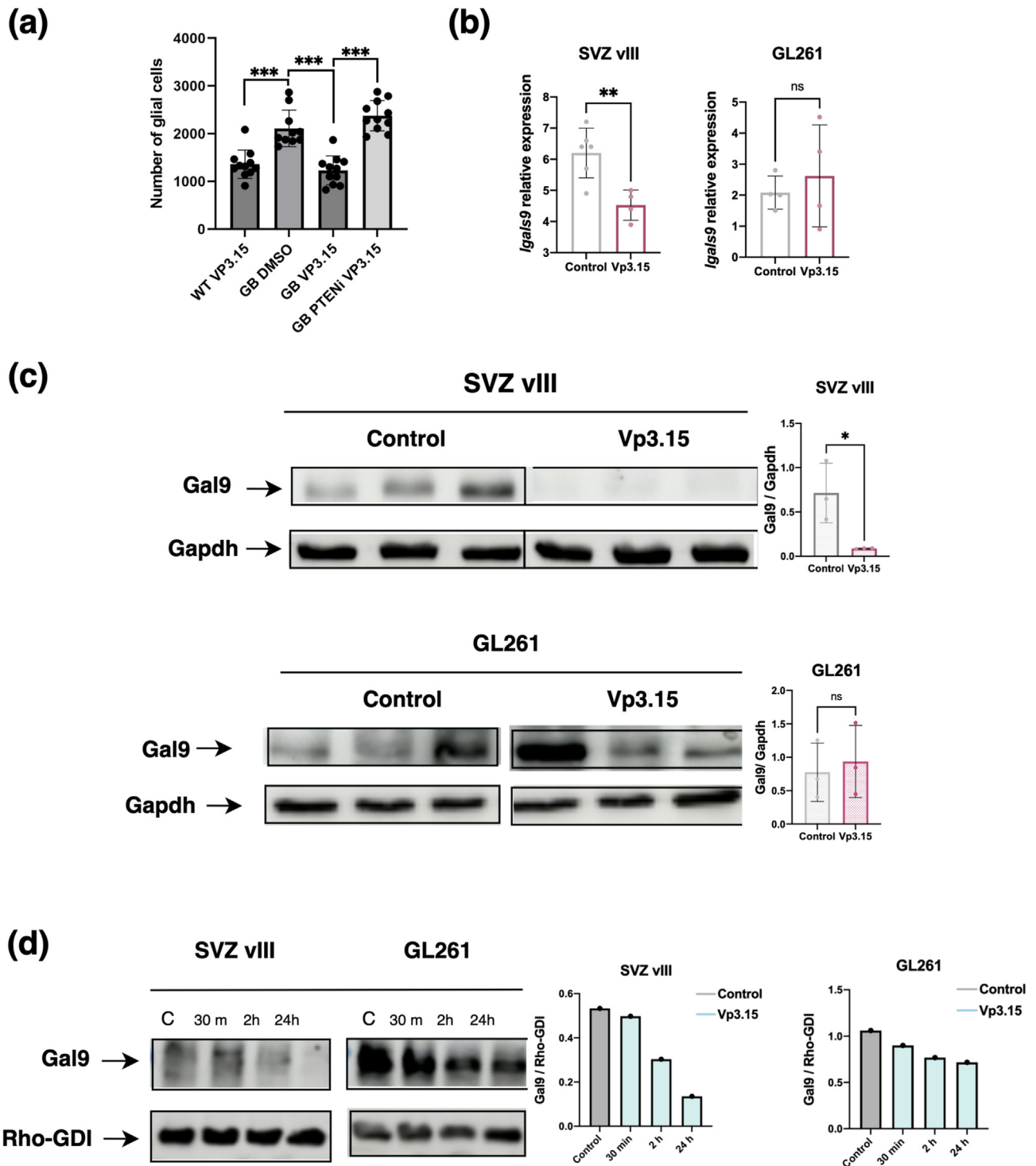


Fig. 6. Analysis of Gal9 expression in response to Vp3.15 treatment in PTEN wild-type and PTEN deficient GB. **a)** Number of glial cells in *Drosophila melanogaster* wild type brain samples treated with VP3.15, GB samples, GB samples treated with VP3.15 and GB *Pten*RNAi samples treated with VP3.15. **b)** qRT-PCR analysis of *Lgals9* expression in SVZ-vIII and GL261 tumors treated with vehicle (Control) or VP3.15. *Actin* expression was used for normalization (n = 5). **c)** Western-Blot (WB) analysis to measure the levels of Gal9 in SVZ-vIII and GL261 tumors treated with vehicle (Control) or VP3.15. Gapdh was used as a loading control. Quantification is shown on the right (n = 3). **d)** SVZ-vIII or GL261 cells were exposed to 1 μ M of VP3.15 for 30min, 2 h and 24 h. Cells were collected and the amount of Gal9 was measured by WB analysis. Rho GDI was used as a loading control. Quantification is shown on the right.

potentially exert a therapeutically negative, pro-survival effect on tumor cells. In addition, some studies have found that GSK-3 β is part of a tumor suppressor complex consisting of Axin and APC that phosphorylates the oncoprotein β -catenin. If GSK-3 β is inactivated, this could potentially lead to tumor promotion [52,53]. Available evidence suggests that GSK-3 β may function as a “tumor suppressor” for certain types of tumors

such as skin and breast tumors [54,55]. These findings suggest that the mechanisms underlying the function of GSK-3 β as a tumor promoter or suppressor may depend on the cell type, tissue context, or, as we propose here, the genetic background of each tumor.

In addition to the inhibiting GSK-3 β , VP3.15 acts as an allosteric inhibitor of PDE7. PDE activity is required in GB cells to promote cell

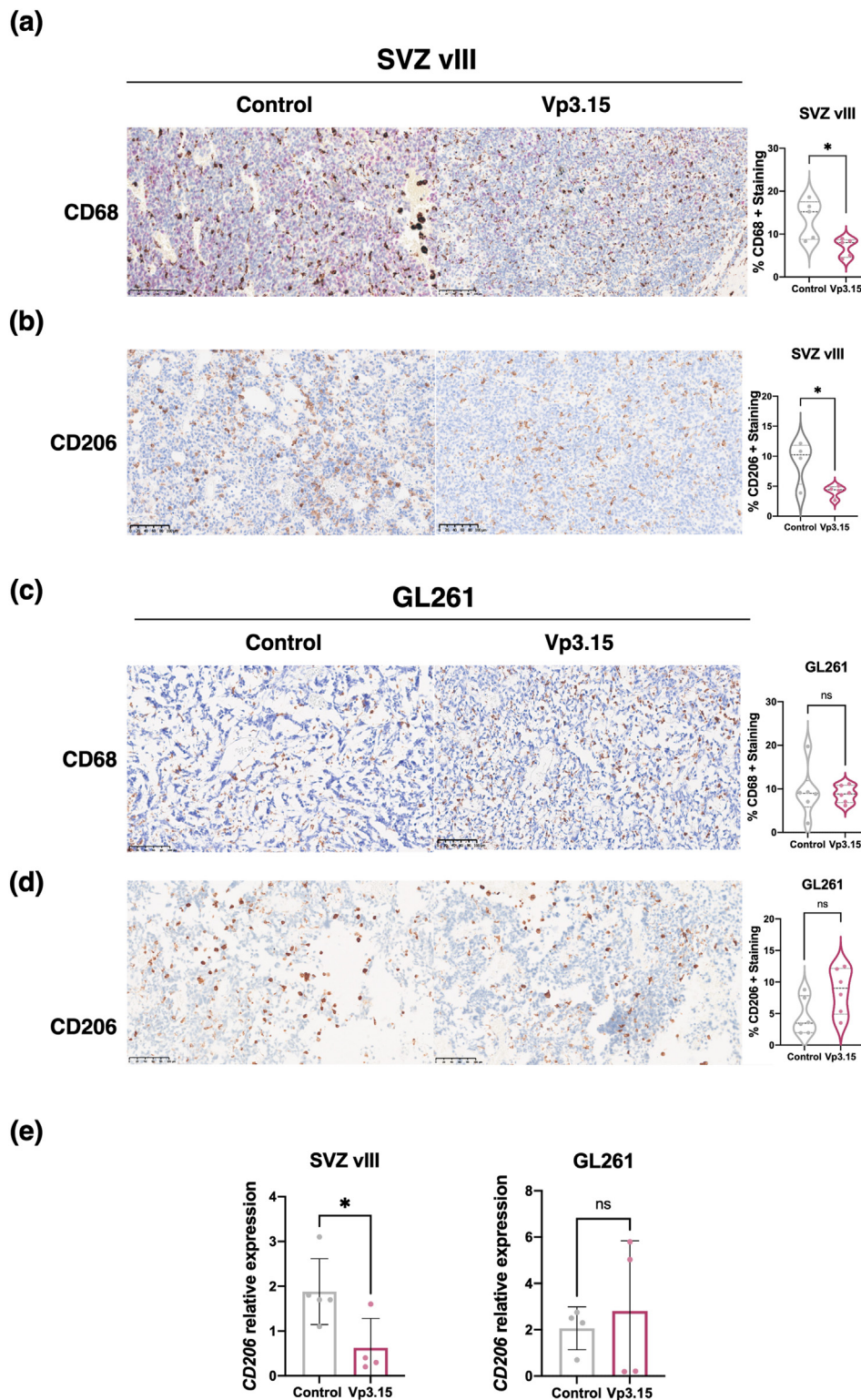


Fig. 7. Analysis of macrophages in response to Vp3.15 treatment in PTEN wild-type and PTEN deficient GB. a-d) Representative images of CD68 (a,c) and CD206 (b,d) staining of SVZ-vIII (a,b) or GL261 (c,d) tumors treated with vehicle (Control) or VP3.15. Quantification is shown on the right. e) qRT-PCR analysis of the expression of CD206 in SVZ-vIII or GL261 tumors treated with vehicle (Control) or VP3.15. Actin was used for normalization. * $P \leq 0.05$. n.s. non-significant. Scale bar: 100 μ M.

proliferation, and therefore the dual inhibitory effect of VP3.15's may address GB progression through two independent flanks. However, PDE7 inhibition also converges on GSK3 β inactivation [43]. Thus, we cannot exclude that the effects of VP3.15 on GB progression are limited to GSK3 β inhibition.

In summary, this study highlights a significant pharmacological profile of VP3.15 as a potential disease-modifying agent for gliomas, demonstrating its strong capacity to reduce immunosuppressive myeloid

infiltration and tumor vascularization. The molecule is orally bioavailable and readily penetrates the blood-brain barrier. These pharmacological properties are particularly encouraging for further development as a drug for adult patients, particularly those with PTENwt gliomas. Nevertheless, the translation of these results into the clinic may open a new avenue to evaluate the efficacy of VP3.15 also in pediatric glioma patients, where Gal9/TIM3 signaling has recently been proven to be a bona fide target [56] and PTEN is rarely mutated. A combination with

anti-angiogenic molecules that have previously failed to block GB growth [4] may also be worth trying. As this molecule disrupts the supportive tumor microenvironment, tumors are likely to be less susceptible to the emergence of resistant subclones with different genetic alterations.

Author contribution statement

Maria Castello-Pons, Investigation, Methodology, Visualization, Writing-review & editing, **Maria A. Ramirez-Gonzalez**, Investigation, Methodology **Patricia Iglesias-Hernández**, Investigation, Methodology, **Nermína Logo Lendo** Investigation. Methodology, **Carlos Rodríguez-Martín** Investigation, Methodology, **Laura Quiralte** Investigation, Methodology, **Juan-Manuel Sepúlveda-Sánchez**, resources, funding acquisition, **Olaya de Dios**, investigation, methodology, visualization, **Carmen Gil**, **Ana Martínez** Conceptualization, Methodology, **Pilar Sánchez-Gómez**, Conceptualization, Methodology, Validation, Formal analysis, Investigation, Resources, Writing Original draft, Writing Review & editing, Visualization, Supervision, Project administration, Funding acquisition and **Sergio Casas-Tinto** Conceptualization, Methodology, Validation, Formal analysis, Investigation, Resources, Writing Original draft, Writing Review & editing, Visualization, Supervision, Project administration, Funding acquisition.

Data availability

All data are available upon request to the corresponding authors.

Declaration of competing interest

The authors declare no competing interests.

Acknowledgments

This work was supported by Ministerio de Ciencia e Innovación and FEDER funds (Instituto de Salud Carlos III): Sara Borrell Contract (CD22CIII/00001) to OdD, AESPI21/01406 to JMS, AESPI21CIII/00002 to PSG, AESPI22CIII/00062 and PID2022-139786OB-I00 to SCT. MCP was supported by the Young Employment Initiative (Comunidad de Madrid).

Appendix A. Supplementary data

Supplementary data to this article can be found online at <https://doi.org/10.1016/j.neurot.2025.e00576>.

References

- [1] Louis DN, Perry A, Reifenberger G, von Deimling A, Figarella-Branger D, Cavenee WK, et al. The 2016 world Health organization classification of tumors of the central nervous system: a summary. *Acta Neuropathol* 2016;131:803–20.
- [2] Gargini R, Segura-Collar B, Sánchez-Gómez P. Cellular plasticity and tumor microenvironment in gliomas: the struggle to hit a moving target. *Cancers* 2020;12:1622.
- [3] Friedmann-Morvinski D, Hambardzumyan D. Monocyte-neutrophil entanglement in glioblastoma. *J Clin Invest* 2023;133:e163451.
- [4] Wang N, Jain RK, Batchelor TT. New directions in anti-angiogenic therapy for glioblastoma. *Neurotherapeutics* 2017;14:321–32.
- [5] Brooks MD, Jackson E, Warrington NM, Luo J, Forsys JT, Taylor S, et al. PDE7B is a novel, prognostically significant mediator of glioblastoma growth whose expression is regulated by endothelial cells. *PLoS One* 2014;9:e107397.
- [6] Zhao P, Li Q, Shi Z, Li C, Wang L, Liu X, et al. GSK-3 β regulates tumor growth and angiogenesis in human glioma cells. *Oncotarget* 2015;6:31901–15.
- [7] Safitri D, Harris M, Potter H, Yan Yeung H, Winfield I, Kopanitsa L, et al. Elevated intracellular cAMP concentration mediates growth suppression in glioma cells. *Biochem Pharmacol* 2020;174:113823.
- [8] Kopanitsa L, Kopanitsa MV, Safitri D, Ladds G, Bailey DS. Suppression of proliferation of human glioblastoma cells by combined phosphodiesterase and multidrug resistance-associated protein 1 inhibition. *Int J Mol Sci* 2021;22:9665.
- [9] Kotliarova S, Pastorino S, Kovell LC, Kotliarov Y, Song H, Zhang W, et al. Glycogen synthase kinase-3 inhibition induces glioma cell death through c-MYC, nuclear factor-kappaB, and glucose regulation. *Cancer Res* 2008;68:6643–51.

- [10] Nowicki MO, Dmitrieva N, Stein AM, Cutter JL, Godlewski J, Saeki Y, et al. Lithium inhibits invasion of glioma cells; possible involvement of glycogen synthase kinase-3. *Neuro Oncol* 2008;10:690–9.
- [11] Aguilar-Morante D, Morales-García JA, Sanz-SanCristobal M, García-Cabezas MA, Santos A, Perez-Castillo A. Inhibition of glioblastoma growth by the thiadiazolidinone compound TDZD-8. *PLoS One* 2010;5:e13879.
- [12] Pyko IV, Nakada M, Sabit H, Teng L, Furuyama N, Hayashi Y, et al. Glycogen synthase kinase 3 β inhibition sensitizes human glioblastoma cells to temozolomide by affecting O6-methylguanine DNA methyltransferase promoter methylation via c-Myc signaling. *Carcinogenesis* 2013;34:2206–17.
- [13] Morales-García JA, Redondo M, Alonso-Gil S, Gil C, Perez C, Martínez A, et al. Phosphodiesterase 7 inhibition preserves dopaminergic neurons in cellular and rodent models of Parkinson disease. *PLoS One* 2011;6:e17240.
- [14] Palomo V, Perez DI, Perez C, Morales-García JA, Soteras I, Alonso-Gil S, et al. 5-imino-1,2,4-thiadiazoles: first small molecules as substrate competitive inhibitors of glycogen synthase kinase 3. *J Med Chem* 2012;55:1645–61.
- [15] Mestre L, Redondo M, Carrillo-Salinas FJ, Morales-García JA, Alonso-Gil S, Pérez-Castillo A, et al. PDE7 inhibitor TC3.6 ameliorates symptomatology in a model of primary progressive multiple sclerosis. *Br J Pharmacol* 2015;172:4277–90.
- [16] Redondo M, Palomo V, Brea J, Pérez DI, Martín-Álvarez R, Pérez C, et al. Identification in silico and experimental validation of novel phosphodiesterase 7 inhibitors with efficacy in experimental autoimmune encephalomyelitis mice. *ACS Chem Neurosci* 2012;3:793–803.
- [17] Casas-Tintó S, Arnés M, Ferrús A. *Drosophila* enhancer-Gal4 lines show ectopic expression during development. *R Soc Open Sci* 2017;4:170039.
- [18] Brand AH, Perrimon N. Targeted gene expression as a means of altering cell fates and generating dominant phenotypes. *Development* 1993;118:401–15.
- [19] Read RD, Cavenee WK, Furnari FB, Thomas JB. A *drosophila* model for EGFR-Ras and PI3K-dependent human glioma. *PLoS Genet* 2009;5:e1000374.
- [20] Portela M, Venkataramani V, Fahey-Lozano N, Seco E, Losada-Perez M, Winkler F, et al. Glioblastoma cells vampirize WNT from neurons and trigger a JNK/MMP signaling loop that enhances glioblastoma progression and neurodegeneration. *PLoS Biol* 2019;17:e3000545.
- [21] Portela M, Segura-Collar B, Argudo I, Sáiz A, Gargini R, Sánchez-Gómez P, et al. Oncogenic dependence of glioma cells on kish/TMEM167A regulation of vesicular trafficking. *Glia* 2019;67:404–17.
- [22] Segura-Collar B, Garranzo-Asensio M, Herranz B, Hernández-SanMiguel E, Cejalvo T, Casas BS, et al. Tumor-derived pericytes driven by EGFR mutations govern the vascular and immune microenvironment of gliomas. *Cancer Res* 2021;81:2142–56.
- [23] Gangoso E, Southgate B, Bradley L, Rus S, Galvez-Cancino F, McGivern N, et al. Glioblastomas acquire myeloid-affiliated transcriptional programs via epigenetic immunoevasion to elicit immune evasion. *Cell* 2021;184:2454–2470.e26.
- [24] Galli R, Binda E, Orfanelli U, Cipelletti B, Gritti A, De Vitis S, et al. Isolation and characterization of tumorigenic, stem-like neural precursors from human glioblastoma. *Cancer Res* 2004;64:7011–21.
- [25] de Dios O, Ramírez-González MA, Gómez-Soria I, Segura-Collar B, Manosalva J, Megías D, et al. NKG2C/KLRC2 tumor cell expression enhances immunotherapeutic efficacy against glioblastoma. *J Immunother Cancer* 2024;12:e009210.
- [26] Yang AC, Vest RT, Kern F, Lee DP, Agam M, Maat CA, et al. A human brain vascular atlas reveals diverse mediators of Alzheimer's risk. *Nature* 2022;603:885–92.
- [27] Abdelfattah N, Kumar P, Wang C, Leu J-S, Flynn WF, Gao R, et al. Single-cell analysis of human glioma and immune cells identifies S100A4 as an immunotherapy target. *Nat Commun* 2022;13:767.
- [28] Korsunsky I, Millard N, Fan J, Slowikowski K, Zhang F, Wei K, et al. Fast, sensitive and accurate integration of single-cell data with Harmony. *Nat Methods* 2019;16:1289–96.
- [29] Shao X, Liao J, Lu X, Xue R, Ai N, Fan X, et al. scCATCH: automatic annotation on cell types of clusters from single-cell RNA sequencing data. *i Sci* 2020;23:100882.
- [30] Ni X, Wu W, Sun X, Ma J, Yu Z, He X, et al. Interrogating glioma-M2 macrophage interactions identifies Gal-9/Tim-3 as a viable target against PTEN-null glioblastoma. *Sci Adv* 2022;8:eabl5165.
- [31] Xu Z-J, Gu Y, Wang C-Z, Jin Y, Wen X-M, Ma J-C, et al. The M2 macrophage marker CD206: a novel prognostic indicator for acute myeloid leukemia. *Oncol Immunology* 2019;9:1683347.
- [32] Palomo V, Perez DI, Perez C, Morales-García JA, Soteras I, Alonso-Gil S, et al. 5-imino-1,2,4-thiadiazoles: first small molecules as substrate competitive inhibitors of glycogen synthase kinase 3. *J Med Chem* 2012;55:1645–61.
- [33] Marchena M, Villarejo-Zori B, Zaldivar-Diez J, Palomo V, Gil C, Hernández-Sánchez C, et al. Small molecules targeting glycogen synthase kinase 3 as potential drug candidates for the treatment of retinitis pigmentosa. *J Enzym Inhib Med Chem* 2017;32:522–6.
- [34] Sánchez-Cruz A, Villarejo-Zori B, Marchena M, Zaldivar-Diez J, Palomo V, Gil C, et al. Modulation of GSK-3 provides cellular and functional neuroprotection in the rd10 mouse model of retinitis pigmentosa. *Mol Neurodegener* 2018;13:19.
- [35] Martín-Álvarez R, Paúl-Fernández N, Palomo V, Gil C, Martínez A, Mengo G. A preliminary investigation of phosphodiesterase 7 inhibitor VP3.15 as therapeutic agent for the treatment of experimental autoimmune encephalomyelitis mice. *J Chem Neuroanat* 2017;80:27–36.
- [36] Benítez-Fernández R, Melero-Jerez C, Gil C, de la Rosa EJ, Martínez A, de Castro F. Dynamics of central remyelination and treatment evolution in a model of multiple sclerosis with optic coherence tomography. *Int J Mol Sci* 2021;22:2440.
- [37] Kotliarova S, Pastorino S, Kovell LC, Kotliarov Y, Song H, Zhang W, et al. Glycogen synthase kinase-3 inhibition induces glioma cell death through c-MYC, nuclear factor-kappaB, and glucose regulation. *Cancer Res* 2008;68:6643–51.
- [38] Nowicki MO, Dmitrieva N, Stein AM, Cutter JL, Godlewski J, Saeki Y, et al. Lithium inhibits invasion of glioma cells; possible involvement of glycogen synthase kinase-3. *Neuro Oncol* 2008;10:690–9.

- [39] Miyashita K, Kawakami K, Nakada M, Mai W, Shakoori A, Fujisawa H, et al. Potential therapeutic effect of glycogen synthase kinase 3beta inhibition against human glioblastoma. *Clin Cancer Res* 2009;15:887–97.
- [40] Korur S, Huber RM, Sivasankaran B, Petrich M, Morin P, Hemmings BA, et al. GSK3beta regulates differentiation and growth arrest in glioblastoma. *PLoS One* 2009;4:e7443.
- [41] Li Y, Lu H, Huang Y, Xiao R, Cai X, He S, et al. Glycogen synthase kinases-3beta controls differentiation of malignant glioma cells. *Int J Cancer* 2010;127:1271–82.
- [42] Shakoori A, Ougolkov A, Yu ZW, Zhang B, Modarressi MH, Billadeau DD, et al. Deregulated GSK3beta activity in colorectal cancer: its association with tumor cell survival and proliferation. *Biochem Biophys Res Commun* 2005;334:1365–73.
- [43] Morales-Garcia JA, Palomo V, Redondo M, Alonso-Gil S, Gil C, Martinez A, et al. Crosstalk between phosphodiesterase 7 and glycogen synthase kinase-3: two relevant therapeutic targets for neurological disorders. *ACS Chem Neurosci* 2014;5:194–204.
- [44] Benítez-Fernández R, Gil C, Guaza C, Mestre L, Martínez A. The dual PDE7-GSK3β inhibitor, VP3.15, as neuroprotective disease-modifying treatment in a model of primary progressive multiple sclerosis. *Int J Mol Sci* 2022;23:14378.
- [45] Medina-Rodríguez EM, Bribián A, Boyd A, Palomo V, Pastor J, Lagares A, et al. Promoting in vivo remyelination with small molecules: a neuroreparative pharmacological treatment for Multiple Sclerosis. *Sci Rep* 2017;7:43545.
- [46] Zhang W, Zhang Y, He Y, Wang X, Fang Q. Lipopolysaccharide mediates time-dependent macrophage M1/M2 polarization through the Tim-3/Galectin-9 signalling pathway. *Exp Cell Res* 2019;376:124–32.
- [47] Wang X, Ding Z, Lin J, Guo Z, Mehta JL. LOX-1 in macrophage migration in response to ox-LDL and the involvement of calpains. *Biochem Biophys Res Commun* 2015;467:135–9.
- [48] Laczko R, Csiszar K. Lysyl Oxidase (LOX): functional contributions to signaling pathways. *Biomolecules* 2020;10:1093.
- [49] Saldanha G. The Hedgehog signalling pathway and cancer. *J Pathol* 2001;193:427–32.
- [50] Waaler J, Machon O, von Kries JP, Wilson SR, Lundenes E, Wedlich D, et al. Novel synthetic antagonists of canonical Wnt signaling inhibit colorectal cancer cell growth. *Cancer Res* 2011;71:197–205.
- [51] Meurette O, Mehlen P. Notch signaling in the tumor microenvironment. *Cancer Cell* 2018;34:536–48.
- [52] Hinoi T, Yamamoto H, Kishida M, Takada S, Kishida S, Kikuchi A. Complex formation of adenomatous polyposis coli gene product and axin facilitates glycogen synthase kinase-3 beta-dependent phosphorylation of beta-catenin and down-regulates beta-catenin. *J Biol Chem* 2000;275:34399–406.
- [53] Rask K, Nilsson A, Brännström M, Carlsson P, Hellberg P, Janson P-O, et al. Wnt-signalling pathway in ovarian epithelial tumours: increased expression of beta-catenin and GSK3beta. *Br J Cancer* 2003;89:1298–304.
- [54] Farago M, Dominguez I, Landesman-Bollag E, Xu X, Rosner A, Cardiff RD, et al. Kinase-inactive glycogen synthase kinase 3beta promotes Wnt signaling and mammary tumorigenesis. *Cancer Res* 2005;65:5792–801.
- [55] Ma C, Wang J, Gao Y, Gao T-W, Chen G, Bower KA, et al. The role of glycogen synthase kinase 3beta in the transformation of epidermal cells. *Cancer Res* 2007;67:7756–64.
- [56] Ausejo-Mauleon I, Labiano S, de la Nava D, Laspidea V, Zalacain M, Marrodán L, et al. TIM-3 blockade in diffuse intrinsic pontine glioma models promotes tumor regression and antitumor immune memory. *Cancer Cell* 2023;41:1911–1926.e8.